

# Reduced Hall carrier density in the overdoped strange metal regime of cuprate superconductors

Carsten Putzke,<sup>1</sup> Siham Benhabib,<sup>2</sup> Wojciech Tabis,<sup>3</sup> Jake Ayres,<sup>1</sup> Zhaosheng

Wang,<sup>4</sup> Liam Malone,<sup>1</sup> Salvatore Licciardello,<sup>5</sup> Jianming Lu,<sup>5</sup> Takeshi Kondo,<sup>6</sup>

Tsunehiro Takeuchi,<sup>7</sup> Nigel E. Hussey,<sup>5</sup> John R. Cooper,<sup>8</sup> and Antony Carrington<sup>1</sup>

<sup>1</sup>*H.H. Wills Physics Laboratory, University of Bristol, Tyndall Avenue, BS8 1TL, United Kingdom*

<sup>2</sup>*Laboratoire National des Champs Magnétiques Intenses (LNCMI-EMFL),*

*(CNRS-INSA-UGA-UPS), Toulouse, 31400, France*

<sup>3</sup>*Laboratoire National des Champs Magnétiques Intenses (LNCMI-EMFL),*

*(CNRS-INSA-UGA-UPS), Toulouse, 31400, France and AGH University of Science and Technology,*

*Faculty of Physics and Applied Computer Science, 30-059 Krakow, Poland.*

<sup>4</sup>*Hochfeld-Magnetlabor Dresden (HLD-EMFL), Helmholtz-Zentrum Dresden-Rossendorf, D-01328 Dresden, Germany*

<sup>5</sup>*High Field Magnet Laboratory (HFML-EMFL) and Institute for Molecules and Materials,*

*Radboud University, Toernooiveld 7, 6525 ED Nijmegen, Netherlands*

<sup>6</sup>*Institute for Solid State Physics, University of Tokyo, Kashiwa-no-ha, Kashiwa, Japan.*

<sup>7</sup>*Toyota Technological Institute, Nagoya 468-8511, Japan.*

<sup>8</sup>*Department of Physics, University of Cambridge,*

*Madingley Road, Cambridge, CB3 0HE, United Kingdom*

Efforts to understand the microscopic origin of superconductivity in the cuprates are dependent on our knowledge of the normal state. The Hall number in the low temperature, high field limit  $n_{\text{H}}(0)$  has a particular significance because within conventional transport theory it is simply related to the number of charge carriers and so its evolution with doping gives crucial information about the nature of the charge transport. Here we report a study of the high field Hall coefficient of the single layer cuprates  $\text{Tl}_2\text{Ba}_2\text{CuO}_{6+\delta}$  (Tl2201) and (Pb/La) doped  $\text{Bi}_2\text{Sr}_2\text{CuO}_{6+\delta}$  (Bi2201) which shows how  $n_{\text{H}}(0)$  evolves in the overdoped, so-called strange metal, phase of cuprates. We find that the hole concentration inferred from  $n_{\text{H}}(0)$  increases smoothly from  $p$  to  $1+p$ , where  $p$  is the number of holes doped into the parent insulating state, over a wide range of the overdoped part of the phase diagram. Surprisingly, this evolution continues beyond the critical hole doping  $p^*$  at which the normal state pseudogap closes. Indeed the evolution of  $n_{\text{H}}$  seems to correlate with the emergence of the anomalous linear-in- $T$  term in the in-plane resistivity rather than the appearance of a pseudogap and reveals a new property of the strange metal regime.

In the search for the microscopic origin of high temperature superconductivity in the cuprates, much effort has been directed to understanding their normal state properties and how these are linked to superconductivity in the temperature-doping phase diagram. In the underdoped regime, several different electronic phases, such as the pseu-

dogap, charge density wave (CDW) and spin density wave phases, are known to exist and cause marked changes in some of the normal state properties [1]. In particular, within the CDW phase at low temperature,  $n_{\text{H}}$  changes sign [2] suggesting some form of Fermi surface reconstruction [3]. In overdoped cuprates, at least beyond the doping level  $p^*$  where the pseudogap closes, there do not appear to be any competing electronic phases and so potentially these provide a simpler starting point from which to understand the emergence of high temperature superconductivity.

In the far overdoped regime, the normal state behavior of Tl2201 resembles, in many aspects, that of a conventional Fermi liquid with coherent quasiparticles around the entire Fermi-surface [4–6], whose shape is found to be well described by conventional density functional theory [7, 8], albeit with a large (factor 3) renormalisation in the effective mass which derives from a narrowing of the band [5, 6]. One aspect of the overdoped regime which contrasts with that of conventional metals is the evolution of the in-plane resistivity  $\rho_{xx}(T)$  with doping.  $\rho_{xx}(T)$  evolves smoothly from linear, close to optimal doping, to quadratic in the far overdoped regime [9, 10] leading to this being called the ‘strange metal’ regime [11, 12].

The close resemblance of the cuprate phase diagram to that of other material families, such as heavy-fermions and iron-pnictides, where superconductivity occurs close to an antiferromagnetic quantum critical point [13] has led to speculation that the linear resistivity close to optimal doping in the cuprates may be a marker for a quantum critical transition to a ‘hidden’ ordered phase [14]. The idea is that quantum fluctuations of the hidden phase provide the scattering mechanism which gives rise to both the linear resistivity and also provide the pairing mechanism for high temperature superconductivity. Possible candidates for this order are the pseudogap or CDW phases, but there is little evidence that either of these phases have a quantum critical end-point [15, 16]. In fact, for both of these phases, the thermodynamic evidence for a true phase transition of any type at finite temperature is weak. For example, there are no observable anomalies in the specific heat [17] as the material is cooled into these phases. On the other hand, a number of recent experiments might support there being a QCP close to optimal doping. First, quantum oscillations in  $\text{YBa}_2\text{Cu}_3\text{O}_{7-\delta}$  (Y123) show that the quasiparticle mass  $m^*$  increases with doping, beyond  $p = 0.12$ , with  $1/m^*$  extrapolating to zero at  $p \sim 0.18$  [18]. Second, measurements of the low- $T$   $R_{\text{H}}$  in Y123 suggest that  $n_{\text{H}}(0)$  undergoes a rapid increase from  $p$  to  $1 + p$  over a narrow doping range  $0.16 < p < 0.20$  [19], revealing possible critical behavior near the pseudogap end point at  $p = p^*$ . Similar behavior has also been seen in Nd-LSCO [20].

Whether such QCP features are generic to all cuprates and whether this QCP is relevant to superconductivity requires further study. Recently, a high-pressure study of  $\text{YBa}_2\text{Cu}_4\text{O}_8$  (Y124) [21] showed that as the maximum  $T_c$  is approached by pressure tuning, rather than by chemical doping,  $m^*$  actually decreases. This suggests that the mass increase in Y123 near optimal doping may be linked to quantum fluctuations in the CDW phase but these fluctuations are not the primary cause of the increase in  $T_c$ . Moreover, interpreting  $n_{\text{H}}(0)$  as a planar hole density may have complications in the systems studied to date. In Y123, the quasi-one-dimensional CuO chains layer increases the  $b$ -axis conductivity but does not contribute to the Hall conductivity, thus increasing the measured  $n_{\text{H}}(0)$  over that expected from the CuO planes alone [19]. In Nd-LSCO,  $p^*$  coincides with a Lifshitz transition [20, 22] that introduces regions of Fermi-surface with electron-like curvature which may also act to increase  $n_{\text{H}}$ .

Here we find that  $n_{\text{H}}(0)$  for two cuprate families, Tl2201 and Bi2201, evolves smoothly as a function of  $p$  right across the overdoped regime so that  $n_{\text{H}}(0)$  does not reach the value  $1+p$  until close to the edge of the superconducting dome. The behavior correlates well with the evolution of the linear component of  $\rho_{xx}(T)$  suggesting that the two have a common origin. Moreover, there does not appear to be a simple correlation between  $n_{\text{H}}(0, p)$  and the closing of the pseudogap as previously conjectured [19, 20].

Tl2201 has unique properties for this study. It has a simple, strongly two-dimensional band-structure with a single CuO layer giving rise to one band crossing the Fermi level. Its maximum  $T_c$  is 94 K and it may be sufficiently overdoped that it becomes non-superconducting yet remains electronically sufficiently clean in the sense that quantum oscillations are observed [4–6]. For the overdoped compositions with  $T_c \lesssim 30$  K, the Fermi surface geometry, scattering rate anisotropy and temperature dependence have all been accurately determined by quantum oscillation, angle-dependent magnetoresistance and angle resolved photoemission (ARPES) measurements [4–8, 23, 24]. Bi2201 is another single-layered cuprate which has a significantly reduced maximum  $T_c$  ( $= 34$  K) and upper critical field ( $H_{c2}$ ), allowing superconductivity to be suppressed over a wider range of field and temperature space thereby reducing uncertainty in  $n_{\text{H}}(0)$ . While quantum oscillations have not been observed in Bi2201, probably because it is less electronically homogenous than Tl2201, its electronic structure has nonetheless been extremely well characterized via ARPES and scanning tunneling microscopy [25–29]. Moreover, Bi2201 can be doped from the strongly overdoped regime (beyond the edge of the superconducting dome) to  $p$  values much less than  $p^*$ , thus allowing the relationship between  $n_{\text{H}}(0)$  and  $p^*$  to be determined.

Single crystals spanning a wide range of doping from strongly overdoped to slightly underdoped were used in this study (see Supplementary Materials for how the effective hole-doping level for each crystal was estimated). Figure 1 shows the field and temperature dependence of the Hall coefficient  $R_{\text{H}}$  for five representative Tl2201 samples. To determine the effective carrier density  $n_{\text{H}}$  from  $R_{\text{H}}$ , we need to analyze the significant field and temperature dependence of  $R_{\text{H}}$  that is evident for all compositions.

Within conventional Boltzmann transport theory, we can calculate the expected field and temperature dependence of  $R_{\text{H}}$  for Tl2201 using the known Fermi surface geometry as well as the anisotropy and  $T$ -dependence of the scattering rate in the Shockley-Chambers tube-integral formula (see SI). At low field,  $R_{\text{H}}$  is enhanced with respect to  $1/ne$  (where  $n$  is the carrier density) due to anisotropy in the Fermi velocity and scattering rate. At high field this anisotropy is averaged out as the electrons complete increasing fractions of their cyclotron orbits before being scattered and consequently  $R_{\text{H}}$  tends toward  $1/ne$  (see Fig. S4). The enhancement in  $R_{\text{H}}$  is reduced at low temperature as scattering becomes dominated by isotropic impurity scattering and this together with the smaller scattering rate means that  $R_{\text{H}}$  approaches  $1/ne$  at lower fields. Higher impurity scattering increases the field scale at which  $R_{\text{H}}$  approaches its infinite field value, but it also considerably diminishes the enhancement over  $1/ne$ , so  $R_{\text{H}} \simeq 1/ne$  at relatively low fields.

For the most overdoped sample of Tl2201 in Fig. 1, with  $T_c = 30$  K,  $R_{\text{H}}$  at high temperature (120 K) decreases slowly with increasing field ( $\sim 10\%$  in 60 T), but as the temperature is lowered, this field dependence becomes weaker

and for  $T \leq 10$  K, it is essentially constant once superconductivity is suppressed ( $\mu_0 H > 20$  T at  $T = 4.2$  K). The limiting value of  $R_H$  at this doping is close to that expected for the Hall number  $n_H \sim 1 + p$ . This limiting behavior is made clearer in the right hand panels of Fig. 1 where  $R_H$  is replotted against  $H/\rho_{xx}^0$  which is proportional to  $\omega_c \tau$ , and reflects the fraction of a cyclotron orbit traversed by an electron before it scatters (here  $\rho_{xx}^0$  is the extrapolated zero field resistivity). The behaviour is very similar to that predicted from conventional Boltzmann transport theory as described above and shown explicitly in the SI.

For the  $T_c = 40$  K sample, at elevated temperatures the  $H$  dependence of  $R_H$  becomes larger but again saturates in the high  $H/T$  limit at a value consistent with  $n_H \sim 1 + p$ . For  $T_c = 65$  K, the irreversibility field has increased significantly. Nevertheless, 60 T still appears to be sufficient to reach the limiting value of  $R_H$ , though in this case, it is found to be significantly higher than that expected from  $n_H \sim 1 + p$ . Indeed, for the optimally doped sample ( $T_c = 90$  K) and the slightly underdoped sample ( $T_c = 85$  K), the values of  $R_H$  at the highest field and lowest temperature correspond more to  $n_H \sim p$  than to  $n_H \sim 1 + p$ .

For Bi2201, the field dependence of  $R_H$ , above  $H_{c2}$ , is much weaker than in Tl2201 (see SI) consistent with a much higher isotropic elastic scattering rate (residual resistivities are almost one order of magnitude larger), and so we would expect the high field/low temperature values of  $n_H$  to more accurately reflect the carrier density.

The  $T$ -dependence of  $n_H$  at fixed high fields, for the different dopings are shown in Figure 2 for both Tl2201 and Bi2201. Extrapolating  $n_H(T)$  to  $T = 0$  for each composition gives  $n_H(0)$  whose evolution with doping is plotted in the lower panels of Figure 3.  $n_H(0)$  is found to evolve smoothly as a function of  $p$  for both single-layered cuprate families. For some doping values, multiple samples were measured and these gave consistent results, giving confidence that the error bars in  $n_H$  are accurate. As for Y123 [19],  $n_H(0)$  for underdoped Tl2201 is of order  $p$  but then increases over a broad doping range until it reaches the  $n_H(0) = 1 + p$  line approximately at the point where  $T_c = 40$  K. In Bi2201, previous measurements have shown that  $n_H(0)$  follows a non-monotonic behavior below  $p^*$  presumably due to the presence of a CDW [30]. In Y123, the CDW causes  $n_H$  to change sign due to Fermi surface reconstruction [2], thus a partial CDW gapping would be expected to substantially increase  $n_H(0)$ . Beyond  $p^*$  however, and across the entire overdoped region of the superconducting dome,  $n_H(0)$  monotonically increases with increasing  $p$  until it coincides with  $1 + p$  near the edge of the superconducting dome. It should be noted that for Bi2201, the location of  $p^*$  can be determined very precisely (at least within this series of samples) from analysis of the temperature derivative  $d\rho_{xx}/dT$ , as described in the SI. For both Tl2201 and Y123,  $n_H(0)$  begins to increase close to optimal doping. The same behaviour is also consistent with an extrapolation of the higher  $p$  data for Bi2201 (Figure 3).

The smooth evolution of  $n_H(0)$  deep into the overdoped regime reveals a new aspect of the strange metal regime in hole-doped cuprates, suggesting it is not necessarily tied to the closing of the normal state pseudogap. This finding thus brings into question whether there is truly a quantum phase transition at  $p^* = 0.19$ . One interpretation of the data is that the decrease in  $n_H(0)$  is related to a pseudogap which does not close abruptly at  $p^*$  but does so gradually over a wide range of doping [31]. As mentioned above, transport signatures of the pseudogap disappear well before  $n_H(0)$  eventually merges with the  $n_H = 1 + p$  line. Thus, at least from a transport perspective, we can be

confident that the decrease in  $n_{\text{H}}(0)$  is taking place over a doping range that exceeds  $p^*$ . In Tl2201, although there is no indication of a pseudogap in either zero field transport [10] or heat capacity measurements [32], it is possible in principle that the pseudogap opens below the zero field  $T_c$ . In this case, assuming that the magnetic field suppresses the superconductivity but not the pseudogap, it would be expected that  $R_{\text{H}}$  would increase as the pseudogap opens, thus decreasing the value of  $n_{\text{H}}$  at low  $T$ . There is no evidence of this from our data as the evolution of  $n_{\text{H}}$  with  $T$  for the  $T_c = 65\text{K}$  sample is very similar, for example, to that for  $T_c = 20\text{K}$ , for which  $n_{\text{H}} \sim 1 + p$  (see Fig. 2). In addition, a pseudogap opening below  $T_c$  would lead to large changes in the superfluid density, being proportional to  $n/m^*$  and heat capacity [33], which are not observed [32, 34].

As discussed above, an enhancement in  $R_{\text{H}}$  can arise due to the presence of anisotropic scattering. In the cuprates, impurity scattering may also be anisotropic [35], arising, for example, when a region of the Fermi surface lies close to a van Hove singularity (vHs). As with anisotropy in the inelastic scattering channel however, any such anisotropy should not influence the extrapolated high-field value of  $R_{\text{H}}$ . Moreover, in Tl2201 in particular, all indications are that the vHs remains above the Fermi level at all doping levels studied (see SI). With decreasing doping, the Fermi level becomes ever further removed from the vHs and as such, the density of states around the Fermi level is expected to become more, not less, isotropic. Thus, such scattering cannot account for the enhancement in  $R_{\text{H}}(0)$  with decreasing doping.

One obvious interpretation of our findings is that the effective number of mobile carriers begins to fall below  $1 + p$  at a doping level close to the edge of the superconducting dome, rather than at  $p^*$ . However, there is no evidence of any marked contraction of the Fermi volume from ARPES measurements in this region of the phase-diagram [36]. Moreover, the superfluid density, increases as optimal doping is approached from the overdoped side [34, 37], implying the opposite trend for the number of superconducting carriers to that of  $n_{\text{H}}(0)$ . Within a Fermi liquid model then, the most likely interpretation of the fall in  $n_{\text{H}}(0)$  is that it evidences an as yet undetected reconstruction of the Fermi surface which begins in the far-overdoped regime. As  $n_{\text{H}}(0)$  is strongly weighted by parts of the Fermi-surface with strong-curvature, reconstruction of the Fermi surface by a density wave can strongly reduce its value.

A more likely interpretation, however, is that the smooth evolution of  $n_{\text{H}}$  with  $p$  evidences a gradual evolution of a Fermi liquid state in the far overdoped regime to an anomalous non-Fermi liquid state for lower doping. Previously, it was shown that  $\rho_{xx}(T)$  in both Tl2201 and  $\text{La}_{2-x}\text{Sr}_x\text{CuO}_4$  could be modelled as the sum of  $T$  and  $T^2$  components [12]. The  $T^2$  (Fermi-liquid like) component remains approximately independent of doping, whereas the anomalous  $T$  component rises almost linearly with  $p$  as  $p$  is decreased from the edge of the superconducting dome [12, 38]. As shown in Figure 3, the reduction of  $n_{\text{H}}(0)$  appears to correlate with the emergence of such a linear-in- $T$  component in  $\rho_{xx}(T)$  in both Tl2201 and Bi2201. Recently, this  $T$ -linear term has been associated with scattering at or close to the so-called Planckian limit that is the maximally allowed rate at which energy can be dissipated [39].

Intriguingly, for Tl2201, the region ( $p > 0.28$ ) where  $n_{\text{H}}(0)$  merges with the  $1 + p$  line is the only region to date in which quantum oscillations have been observed [5]. Although there could be several reasons [6] why quantum oscillations were not observed for higher  $T_c$  samples, such as increased impurity scattering, in the light of these new

results it is plausible that the loss of quasiparticle coherence around the Fermi surface is preventing quantum oscillatory phenomena from being realized. The quasi-classical model of angle-dependent, out-of-plane magnetoresistance, so successful in modelling the lower  $T_c$  samples of Tl2201, also fails around this doping,  $T_c \sim 40$  K, suggesting the advent of additional scattering or decoherence [40]. Although a density wave reconstruction for  $p < 0.28$  might explain the decrease in  $n_H(0)$ , this should also give rise to small Fermi pockets which should exhibit quantum oscillations. Their non-observation coupled with the absence of anomalies in the specific heat [32], suggests that decoherence associated with non-Fermi liquid behaviour is a more likely scenario to explain all these phenomena. The findings presented here show that the evolution of the normal state electronic properties stretch over a wide range of the overdoped phase diagram. The endpoint of this transition in  $n_H(0)$  appears closely linked to optimal doping in agreement with other systems [19, 20]. The simultaneous evolution of decoherence in the normal state properties and the concomitant increase in  $T_c$  across the overdoped region of the phase diagram, that culminates in a maximum  $T_c$  and the development of instabilities in the normal state properties emphasizes how closely the two phenomena are linked. Identifying how the decoherence influences the Hall response might then help us in the quest to better understand superconductivity in the hole-doped cuprates.

- 
- [1] B. Keimer, S. A. Kivelson, M. R. Norman, S. Uchida, and J. Zaanen, From quantum matter to high-temperature superconductivity in copper oxides, *Nature* **518**, 179 (2015).
  - [2] D. LeBoeuf, N. Doiron-Leyraud, J. Levallois, R. Daou, J. B. Bonnemaïson, N. E. Hussey, L. Balicas, B. J. Ramshaw, R. X. Liang, D. A. Bonn, W. N. Hardy, S. Adachi, C. Proust, and L. Taillefer, Electron pockets in the fermi surface of hole-doped high- $t_c$  superconductors, *Nature* **450**, 533 (2007).
  - [3] S. E. Sebastian, N. Harrison, and G. G. Lonzarich, Towards resolution of the fermi surface in underdoped high- $t_c$  superconductors, *Rep. Prog. Phys.* **75**, 102501 (2012).
  - [4] B. Vignolle, A. Carrington, R. A. Cooper, M. M. J. French, A. P. Mackenzie, C. Jaudet, D. Vignolles, C. Proust, and N. E. Hussey, Quantum oscillations in an overdoped high- $t_c$  superconductor, *Nature* **455**, 952 (2008).
  - [5] A. F. Bangura, P. M. C. Rourke, T. M. Benseman, M. Matusiak, J. R. Cooper, N. E. Hussey, and A. Carrington, Fermi surface and electronic homogeneity of the overdoped cuprate superconductor  $\text{tl}_2\text{ba}_2\text{cuo}_{6+\delta}$  as revealed by quantum oscillations, *Phys. Rev. B* **82**, 140501 (2010).
  - [6] P. M. C. Rourke, A. F. Bangura, T. M. Benseman, M. Matusiak, J. R. Cooper, A. Carrington, and N. E. Hussey, A detailed de haas-van alphen effect study of the overdoped cuprate  $\text{tl}_2\text{ba}_2\text{cuo}_{6+\delta}$ , *New J. Phys.* **12**, 105009 (2010).
  - [7] N. E. Hussey, M. Abdel-Jawad, A. Carrington, A. P. Mackenzie, and L. Balicas, A coherent three-dimensional fermi surface in a high-transition-temperature superconductor, *Nature* **425**, 814 (2003).
  - [8] M. Plate, J. D. F. Mottershead, I. S. Elfimov, D. C. Peets, R. Liang, D. A. Bonn, W. N. Hardy, S. Chiuzbaian, M. Falub, M. Shi, L. Patthey, and A. Damascelli, Fermi surface and quasiparticle excitations of overdoped  $\text{tl}_2\text{ba}_2\text{cuo}_{6+\delta}$ , *Phys. Rev. Lett.* **95**, 077001 (2005).
  - [9] Y. Kubo, Y. Shimakawa, T. Manako, and H. Igarashi, Transport and magnetic-properties of  $\text{tl}_2\text{ba}_2\text{cuo}_{6+\delta}$  showing a delta-dependent gradual transition from an 85k superconductor to a nonsuperconducting metal, *Phys. Rev. B* **43**, 7875 (1991).

- [10] T. Manako, Y. Kubo, and Y. Shimakawa, Transport and structural study of  $\text{tl}_2\text{ba}_2\text{cuo}_{6+\delta}$  single-crystals prepared by the kcl flux method, *Phys. Rev. B* **46**, 11019 (1992).
- [11] N. E. Hussey, Phenomenology of the normal state in-plane transport properties of high- $t_c$  cuprates, *J. Phys.-Condens. Matter* **20**, 123201 (2008).
- [12] N. E. Hussey, H. Gordon-Moys, J. Kokalj, and R. H. McKenzie, Generic strange-metal behaviour of overdoped cuprates, *J. Phys.: Conf. Ser.* **449**, 012004 (2013).
- [13] T. Shibauchi, A. Carrington, and Y. Matsuda, A quantum critical point lying beneath the superconducting dome in iron pnictides, *Annu. Rev. Condens. Matter Phys.* **5**, 113 (2014).
- [14] L. Taillefer, Scattering and pairing in cuprate superconductors, *Annu. Rev. Condens. Matter Phys.* **1**, 51 (2010).
- [15] S. Blanco-Canosa, A. Frano, E. Schierle, J. Porras, T. Loew, M. Minola, M. Bluschke, E. Weschke, B. Keimer, and M. Le Tacon, Resonant x-ray scattering study of charge-density wave correlations in  $\text{yba}_2\text{cu}_3\text{o}_{6+x}$ , *Phys. Rev. B* **90**, 054513 (2014).
- [16] W. Tabis, B. Yu, I. Bialo, M. Bluschke, T. Kolodziej, A. Kozłowski, E. Blackburn, K. Sen, E. M. Forgan, M. v. Zimmermann, Y. Tang, E. Weschke, B. Vignolle, M. Hepting, H. Gretarsson, R. Sutarto, F. He, M. Le Tacon, N. Barišić, G. Yu, and M. Greven, Synchrotron x-ray scattering study of charge-density-wave order in  $\text{hgba}_2\text{cuo}_{4+\delta}$ , *Phys. Rev. B* **96**, 134510 (2017).
- [17] J. R. Cooper, J. W. Loram, I. Kokanovic, J. G. Storey, and J. L. Tallon, Pseudogap in  $\text{yba}_2\text{cu}_3\text{o}_{6+\delta}$  is not bounded by a line of phase transitions: Thermodynamic evidence, *Phys. Rev. B* **89**, 201104 (2014).
- [18] B. J. Ramshaw, S. E. Sebastian, R. D. McDonald, J. Day, B. S. Tan, Z. Zhu, J. B. Betts, R. X. Liang, D. A. Bonn, W. N. Hardy, and N. Harrison, Quasiparticle mass enhancement approaching optimal doping in a high- $t_c$  superconductor, *Science* **348**, 317 (2015).
- [19] S. Badoux, W. Tabis, F. Laliberte, G. Grissonnanche, B. Vignolle, D. Vignolles, J. Beard, D. A. Bonn, W. N. Hardy, R. Liang, N. Doiron-Leyraud, L. Taillefer, and C. Proust, Change of carrier density at the pseudogap critical point of a cuprate superconductor, *Nature* **531**, 210 (2016).
- [20] C. Collignon, S. Badoux, S. A. A. Afshar, B. Michon, F. Laliberte, O. Cyr-Choiniere, J. S. Zhou, S. Licciardello, S. Wiedmann, N. Doiron-Leyraud, and L. Taillefer, Fermi-surface transformation across the pseudogap critical point of the cuprate superconductor  $\text{la}_{1.6-x}\text{nd}_{0.4}\text{sr}_x\text{cuo}_4$ , *Phys. Rev. B* **95**, 224517 (2017).
- [21] C. Putzke, L. Malone, S. Badoux, B. Vignolle, D. Vignolles, W. Tabis, P. Walmsley, M. Bird, N. E. Hussey, C. Proust, and A. Carrington, Inverse correlation between quasiparticle mass and  $t_c$  in a cuprate high- $t_c$  superconductor, *Sci. Adv.* **2**, e1501657 (2016).
- [22] C. E. Matt, C. G. Fatuzzo, Y. Sassa, M. Månsson, S. Fatale, V. Bitetta, X. Shi, S. Pailhès, M. H. Berntsen, T. Kurosawa, M. Oda, N. Momono, O. J. Lipscombe, S. M. Hayden, J.-Q. Yan, J.-S. Zhou, J. B. Goodenough, S. Pyon, T. Takayama, H. Takagi, L. Patthey, A. Bendounan, E. Razzoli, M. Shi, N. C. Plumb, M. Radovic, M. Grioni, J. Mesot, O. Tjernberg, and J. Chang, Electron scattering, charge order, and pseudogap physics in  $\text{la}_{1.6-x}\text{nd}_{0.4}\text{sr}_x\text{cuo}_4$ : An angle-resolved photoemission spectroscopy study, *Phys. Rev. B* **92**, 134524 (2015).
- [23] M. Abdel-Jawad, M. P. Kennett, L. Balicas, A. Carrington, A. P. Mackenzie, R. H. McKenzie, and N. E. Hussey, Anisotropic scattering and anomalous normal-state transport in a high-temperature superconductor, *Nat. Phys.* **2**, 821 (2006).
- [24] M. Abdel-Jawad, J. G. Analytis, L. Balicas, A. Carrington, J. P. H. Charmant, M. M. J. French, and N. E. Hussey, Correlation between the superconducting transition temperature and anisotropic quasiparticle scattering in  $\text{tl}_2\text{ba}_2\text{cuo}_{6+\delta}$ , *Phys. Rev. Lett.* **99**, 107002 (2007).

- [25] T. Kondo, T. Takeuchi, U. Mizutani, T. Yokoya, S. Tsuda, and S. Shin, Contribution of electronic structure to thermoelectric power in  $(\text{Bi,Pb})_2(\text{Sr,L a})_2\text{CuO}_{6+\delta}$ , *Phys. Rev. B* **72**, 024533 (2005).
- [26] T. Kondo, T. Takeuchi, A. Kaminski, Y. Tsuda, and S. Shin, Evidence for two energy scales in the superconducting state of optimally doped  $(\text{Bi,Pb})_2(\text{Sr,L a})_2\text{CuO}_{6+\delta}$ , *Phys. Rev. Lett.* **98**, 267004 (2007).
- [27] W. D. Wise, M. C. Boyer, K. Chatterjee, T. Kondo, T. Takeuchi, H. Ikuta, Y. Wang, and E. W. Hudson, Charge-density-wave origin of cuprate checkerboard visualized by scanning tunnelling microscopy, *Nat. Phys.* **4**, 696 (2008).
- [28] W. D. Wise, K. Chatterjee, M. C. Boyer, T. Kondo, T. Takeuchi, H. Ikuta, Z. Xu, J. Wen, G. D. Gu, Y. Wang, and E. W. Hudson, Imaging nanoscale fermi-surface variations in an inhomogeneous superconductor, *Nat. Phys.* **5**, 213 (2009).
- [29] T. Kondo, R. Khasanov, T. Takeuchi, J. Schmalian, and A. Kaminski, Competition between the pseudogap and superconductivity in the high- $t_c$  copper oxides, *Nature* **457**, 296 (2009).
- [30] F. Balakirev, J. Betts, A. Migliori, S. Ono, Y. Ando, and G. Boebinger, Signature of optimal doping in hall-effect measurements on a high-temperature superconductor, *Nature* **424**, 912 (2003).
- [31] D. Pelc, P. Popčević, M. Požek, M. Greven, and N. Barišić, Unusual behavior of cuprates explained by heterogeneous charge localization, *Science Advances* **5**, eaau4538 (2019).
- [32] J. M. Wade, J. W. Loram, K. A. Mirza, J. R. Cooper, and J. L. Tallon, Electronic specific-heat of  $\text{tl}_2\text{ba}_2\text{cuo}_{6+\delta}$  from 2 k to 300 k for  $0 \geq \delta \geq 0.1$ , *J. Supercond.* **7**, 261 (1994).
- [33] J. M. Tallon, J. G. Storey, J. R. Cooper, and J. W. Loram, Locating the pseudogap closing point in cuprate superconductors: absence of entrant or reentrant behavior, *arXiv:1907.12018* (2019).
- [34] D. M. Broun, D. C. Morgan, R. J. Ormeno, S. F. Lee, A. W. Tyler, A. P. Mackenzie, and J. R. Waldram, In-plane microwave conductivity of the single-layer cuprate  $\text{tl}_2\text{ba}_2\text{cuo}_{6+\delta}$ , *Phys. Rev. B* **56**, R11443 (1997).
- [35] E. Abrahams and C. M. Varma, Hall effect in the marginal fermi liquid regime of high- $t_c$  superconductors, *Phys. Rev. B* **68**, 094502 (2003).
- [36] Y. Ding, L. Zhao, H.-T. Yan, Q. Gao, J. Liu, C. Hu, J.-W. Huang, C. Li, Y. Xu, Y.-Q. Cai, H.-T. Rong, D.-S. Wu, C.-Y. Song, H.-X. Zhou, X.-L. Dong, G.-D. Liu, Q.-Y. Wang, S.-J. Zhang, Z.-M. Wang, F.-F. Zhang, F. Yang, Q.-J. Peng, Z.-Y. Xu, C.-T. Chen, and X. J. Zhou, Disappearance of superconductivity and a concomitant lifshitz transition in heavily overdoped  $\text{bi}_2\text{sr}_2\text{cuo}_6$  superconductor revealed by angle-resolved photoemission spectroscopy, *Chinese Phys. Lett.* **36**, 017402 (2019).
- [37] D. Deepwell, D. C. Peets, C. J. S. Truncik, N. C. Murphy, M. P. Kennett, W. A. Huttema, R. Liang, D. A. Bonn, W. N. Hardy, and D. M. Broun, Microwave conductivity and superfluid density in strongly overdoped  $\text{tl}_2\text{ba}_2\text{cuo}_{6+\delta}$ , *Phys. Rev. B* **88**, 214509 (2013).
- [38] R. A. Cooper, Y. Wang, B. Vignolle, O. J. Lipscombe, S. M. Hayden, Y. Tanabe, T. Adachi, Y. Koike, M. Nohara, H. Takagi, C. Proust, and N. E. Hussey, Anomalous criticality in the electrical resistivity of  $\text{la}_{2-x}\text{sr}_x\text{cuo}_4$ , *Science* **323**, 603 (2009).
- [39] A. Legros, S. Benhabib, W. Tabis, F. Laliberte, M. Dion, M. Lizaire, B. Vignolle, D. Vignolles, H. Raffy, Z. Z. Li, P. Auban-Senzier, N. Doiron-Leyraud, P. Fournier, D. Colson, L. Taillefer, and C. Proust, Universal t-linear resistivity and planckian dissipation in overdoped cuprates, *Nature Physics* **15**, 142 (2019).
- [40] M. M. J. French, J. G. Analytis, A. Carrington, L. Balicas, and N. E. Hussey, Tracking anisotropic scattering in overdoped  $\text{tl}_2\text{ba}_2\text{cuo}_{6+\delta}$  above 100 k, *New J. Phys.* **11**, 055057 (2009).
- [41] A. P. Mackenzie, S. R. Julian, D. C. Sinclair, and C. T. Lin, Normal-state magnetotransport in superconducting  $\text{tl}_2\text{ba}_2\text{cuo}_{6+\delta}$  to millikelvin temperatures, *Phys. Rev. B* **53**, 5848 (1996).
- [42] A.W. Tyler, An Investigation into the Magnetotransport Properties of Layered Superconducting Perovskites. Ph.D. thesis,

University of Cambridge (1997).

[43] R. Liang, D. A. Bonn, and W. N. Hardy, Evaluation of  $\text{CuO}_2$  plane hole doping in  $\text{YBa}_2\text{Cu}_3\text{O}_{6+x}$  single crystals, *Phys. Rev. B* **73**, 180505 (2006).

[44] M. French, PhD Thesis University of Bristol (2009).

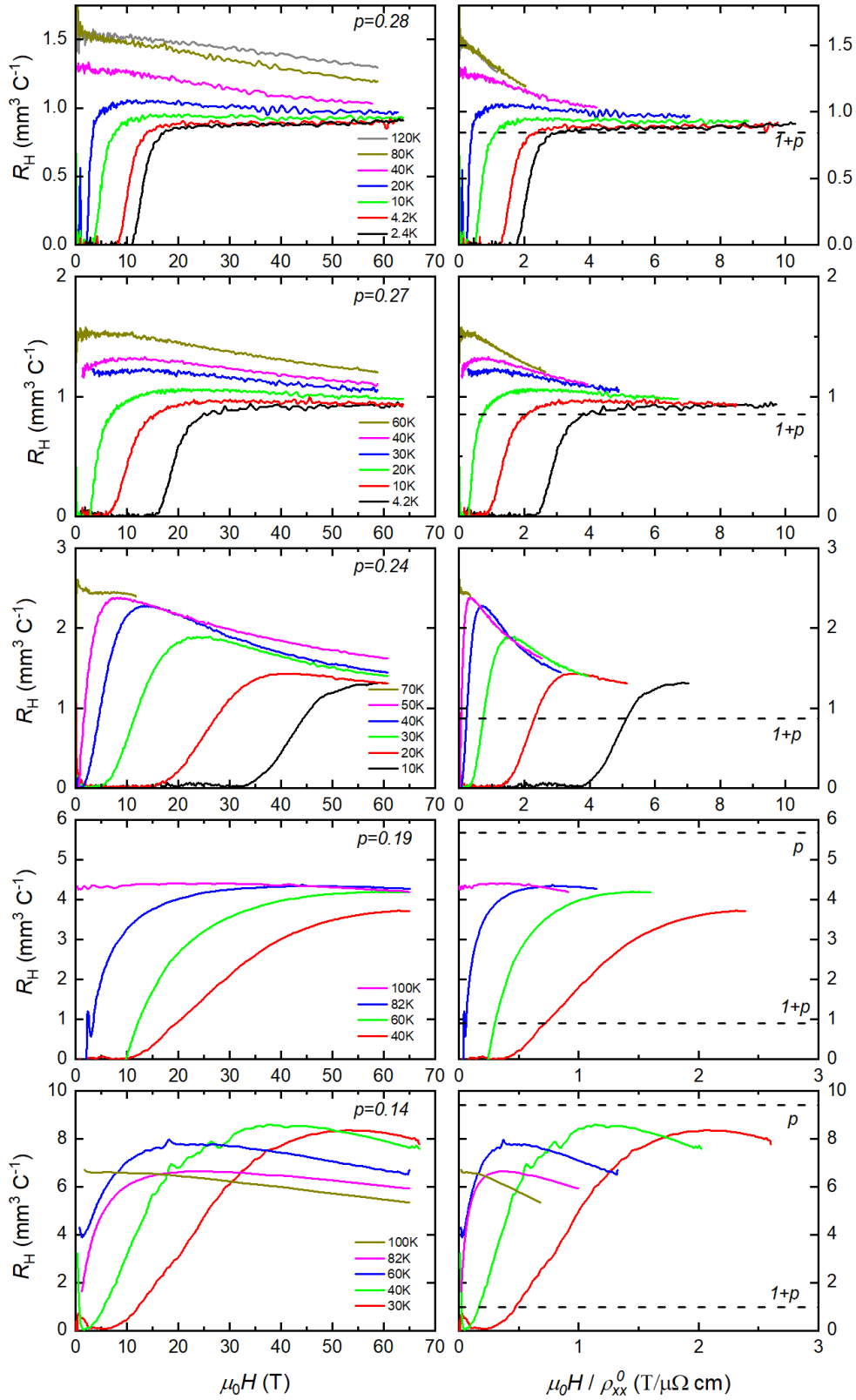


FIG. 1: Field dependence of the Hall coefficient  $R_H$  for samples of Tl2201 with various doping levels. The left hand panels show the raw data at different temperatures and the right panels show the same data with the field scaled by the estimated value of the resistivity  $\rho(T)$  at  $H = 0$ . The dashed lines show the  $R_H$  values corresponding to  $1/n_H$  where  $n_H = 1 + p$  and  $n_H = p$ .

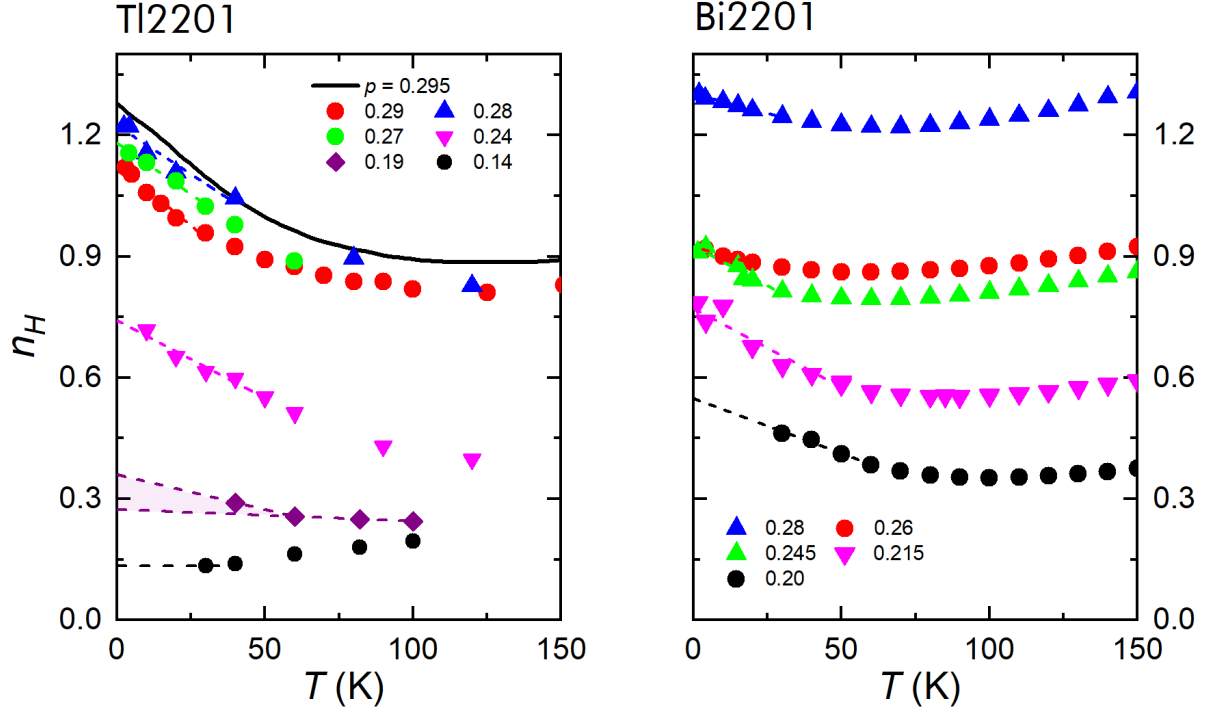


FIG. 2: Evolution of the Hall number  $n_H$  with temperature for samples of Tl2201 and Bi2201 with different doping values  $p$  as indicated.  $n_H$  values are taken at the highest values of field ( $\mu_0 H = 60$  to  $65$  T) in Figure 1). The dashed lines show the extrapolation to  $T = 0$  to give  $n_H(0)$ . For the sample with  $p = 0.19$  we show two possible extrapolations. The solid line shows  $n_H(T)$  for a  $T_c = 15$  K sample of Tl2201 taken from Ref. [41], with  $\mu_0 H = 16$  T.

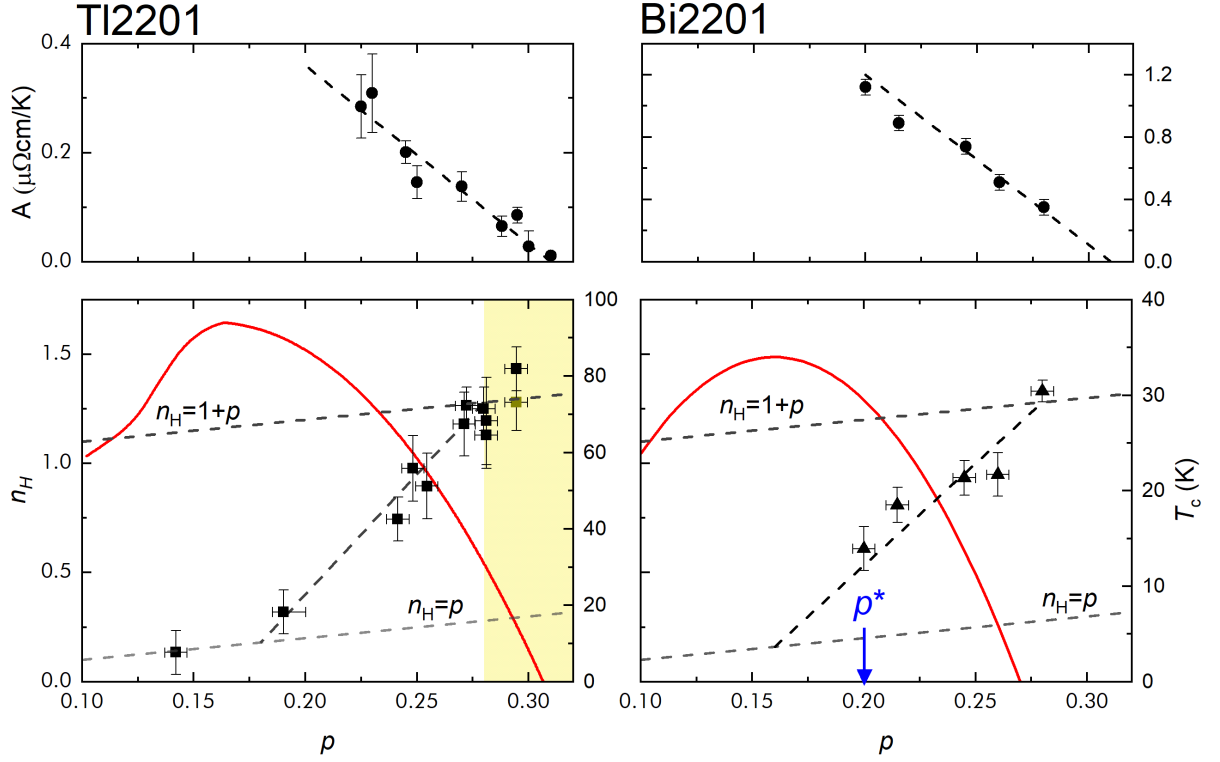


FIG. 3: Bottom panel: High field and low temperature values of the Hall number  $n_H(0)$  versus doped holes ( $p$ ) for Tl2201 and Bi2201, from the extrapolations shown in Figure 2. The data point for the most overdoped sample is taken from Ref. [41]. The grey dashed lines show the behavior expected for  $n_H(0) = p$  and  $n_H(0) = 1 + p$  and the black dashed line is a guide for the eye. The error bars in  $n_H$  reflect the geometric uncertainty, whereas those for  $p$  reflect the uncertainty in  $T_c$ . The assumed evolution of  $T_c(p)$  is shown with a solid red line for each compound (right hand scale, see SI). The shaded area on the Tl2201 panel shows the doping range where quantum oscillations have been observed. The end of the pseudogap phase ( $p^*$ ) is indicated ( $0.20 < p < 0.215$ ). Top Panels: Evolution of linear-in- $T$  coefficient of the zero field resistivity of Tl2201 [12] and Bi2201. The  $A$  error bars reflect the geometric uncertainty.

## Methods

### Sample preparation and characterization

**Tl2201** Single crystals of Tl2201 were grown by a self flux technique using a similar technique to that described in Ref. [42]. We used a  $\text{ZrO}_2$  crucible with a lid attached rigidly using a fused quartz holder to reduce Tl loss at high temperatures. The samples are tetragonal with a small Cu excess and Tl deficiency.

Very thin platelet-like samples were selected, and annealed in either vacuum or an oxygen/nitrogen gas mixture for between 30 minutes and 4 hours to set the oxygen level. Details are shown in Table S1. Following the anneal, the samples were removed from the furnace and cooled rapidly in the same atmosphere. Rapid cooling was facilitated by an aluminum heat sink around the quartz tube. Contacts were applied by sputtering Au pads onto the top and sides of the samples using a mask. Gold wires were attached to the pads using Dupont 4929 silver paint which was and dried at room temperature for a least one hour, prior to the oxygen-setting annealing process.

Measurements of  $R_H$  were performed in pulsed field either at the LNCMI in Toulouse or the HLD in Dresden using a numerical lock-in digitization technique operating around 50 kHz. For each temperature point measurements were made with the field both parallel or antiparallel to the  $c$ -axis. The Hall resistance  $R_{xy}$  was then calculated from the odd part of the magnetoresistance and the Hall number  $n_H = V_{\text{cell}}/(eR_H)$  using the cell parameters  $a = 3.87\text{\AA}$ ,  $c = 11.6\text{\AA}$  which gives the cell volume appropriate for one formula unit of Tl2201. Resistance versus temperature curves were measured in zero field by a standard 4 probe technique using a lock-in amplifier at 72 Hz, and were used to determine  $T_c$  of the samples which we define as the temperature where the resistance falls to 1% of the value just above  $T_c$ .

For Fig. 1, in the main text, to estimate the value of the resistivity  $\rho(T)$  at  $H = 0$  without the influence of superconductivity, we used the relation  $\rho(T) = AT + BT^2 + \rho(0)$  with doping dependent coefficients  $A(p), B(p)$  taken from the analysis in Ref. [12].

Sample	$T_c$	doping	thickness	Anneal Conditions
C1	85 K	0.14	25 $\mu\text{m}$	550°C, $10^{-5}$ mbar
C2	90 K	0.19	15 $\mu\text{m}$	500°C, $10^{-3}$ mbar
C15	65 K	0.24	8 $\mu\text{m}$	550°C, 2% O <sub>2</sub> in N <sub>2</sub>
678-10	60 K	0.25	18 $\mu\text{m}$	520°C, 2% O <sub>2</sub> in N <sub>2</sub>
C7	55 K	0.26	13 $\mu\text{m}$	500°C, 2% O <sub>2</sub> in N <sub>2</sub>
C24	40 K	0.27	16 $\mu\text{m}$	450°C, 2% O <sub>2</sub> in N <sub>2</sub>
C23	39 K	0.27	30 $\mu\text{m}$	450°C, 2% O <sub>2</sub> in N <sub>2</sub>
J3	30 K	0.28	18 $\mu\text{m}$	450°C, 2% O <sub>2</sub> in N <sub>2</sub>
678-19	30 K	0.28	20 $\mu\text{m}$	450°C, 2% O <sub>2</sub> in N <sub>2</sub>
C20	31 K	0.28	15 $\mu\text{m}$	450°C, 20% O <sub>2</sub> in N <sub>2</sub>
C8	30 K	0.28	15 $\mu\text{m}$	450°C, 20% O <sub>2</sub> in N <sub>2</sub>
C22	15 K	0.30	50 $\mu\text{m}$	450°C, 100% O <sub>2</sub>

Table S I: Physical details of the Tl2201 samples studied.

The doping level of the samples was estimated from the measured  $T_c$ . Conventionally, the parabolic relationship

$1 - T_c/T_{c,\max} = 82.6(p - 0.16)^2$  is used to relate  $T_c$  to  $p$ , where  $T_{c,\max}$  differs between compounds, but universally predicts that  $T_c = 0$  at  $p = 0.27$ . This derives from data for  $\text{La}_{2-x}\text{Sr}_x\text{CuO}_4$ , where  $x$  is thought to be equal to  $p$ . For Tl2201 precise measurements of the Fermi surface volume are available from quantum oscillation measurements, and it is found that  $p = 0.30$  for  $T_c = 10$  K which is a doping level considerably larger than that predicted by the above relation [4–6] possibly because  $T_c$  is reduced by disorder rather than doping in strongly overdoped  $\text{La}_{2-x}\text{Sr}_x\text{CuO}_4$ . For this reason, for the overdoped region we used  $1 - T_c/T_{c,\max} = 46.5(p - 0.16)^2$  with  $T_{c,\max} = 94$  K which accounts for the larger doping range of superconductivity in Tl2201 but retains the fixed point  $p = 0.16$  for optimal doping.

For the sample with  $T_c = 85$  K there is potential ambiguity as the  $p$  value depends on whether this is underdoped or overdoped. It was annealed at a higher temperature and higher vacuum level than the  $T_c = 90$  K sample, both of which would be expected to produce a lower doping. The  $\rho(T)$  data for this sample may also indicate underdoping as there is significant downward curvature close to  $T_c$  and the absolute magnitude is higher than the  $T_c = 90$  K sample at room temperature (Fig. S4). The downward curvature could suggest the presence of a pseudogap but could also be caused by superconducting fluctuations [33]. We therefore determined the doping of this sample ( $p = 0.142$ ) to be the same as for  $\text{YBa}_2\text{Cu}_3\text{O}_{7-\delta}$  [43] with the same  $T_c$  value (note  $T_{c,\max}$  for  $\text{YBa}_2\text{Cu}_3\text{O}_{7-\delta}$  is 93.6 K which is virtually identical to that of Tl2201). If the sample were instead overdoped, the doping would be  $p = 0.205$ , which would move the point just to the right of the 90 K point in Fig. 3. This would not affect our conclusions significantly.

**Bi2201** Single crystal samples of Bi2201 doped with both Pb and La, with general formula  $\text{Bi}_{2-y+z}\text{Pb}_y\text{Sr}_{2-x-z}\text{La}_x\text{CuO}_{6+\delta}$ , were grown using the floating zone technique. Samples grown in the same manner in the same laboratory have previously been studied using ARPES and STM. Table S2 lists the stoichiometry of each of our samples as well as the annealing conditions. Also listed are the  $T_c$  values as determined from their resistive transitions. Contacts were applied by gluing gold wires onto freshly cleaved surfaces using Dupont 6838

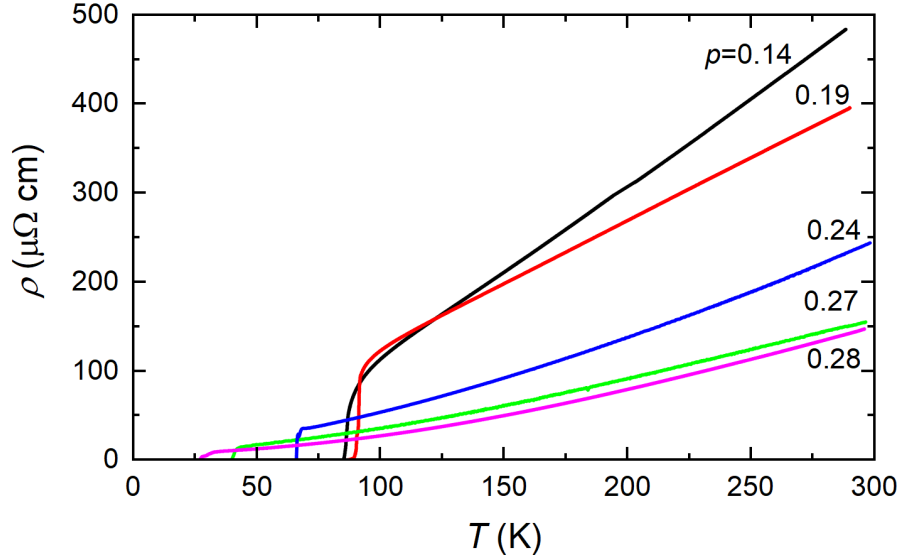


Fig. S 4: Measured temperature dependence of the resistivity for the samples of Tl2201.

$T_c$	doping	thickness	Bi	Pb	Sr	La	Anneal Conditions
29.1 K	0.20	6.4 $\mu\text{m}$	1.20	0.90	1.30	0.55	As grown
25.8 K	0.215	18 $\mu\text{m}$	1.35	0.85	1.47	0.38	650°C, 72 h in 1 atm. N <sub>2</sub>
14.5 K	0.245	27 $\mu\text{m}$	1.72	0.38	1.85	0.0	550°C, 72 h in 1 atm. N <sub>2</sub>
6.8 K	0.26	25 $\mu\text{m}$	1.72	0.38	1.85	0.0	750°C, 24 h in 1 atm. 20%O <sub>2</sub> /N <sub>2</sub>
< 2 K	0.28	44 $\mu\text{m}$	1.72	0.38	1.85	0.0	400°C, 86 h in 2.5 atm. O <sub>2</sub>

Table S II: Physical details of the Bi2201 samples studied, with general formula  $\text{Bi}_{2-y+z}\text{Pb}_y\text{Sr}_{2-x-z}\text{La}_x\text{CuO}_{6+\delta}$ .

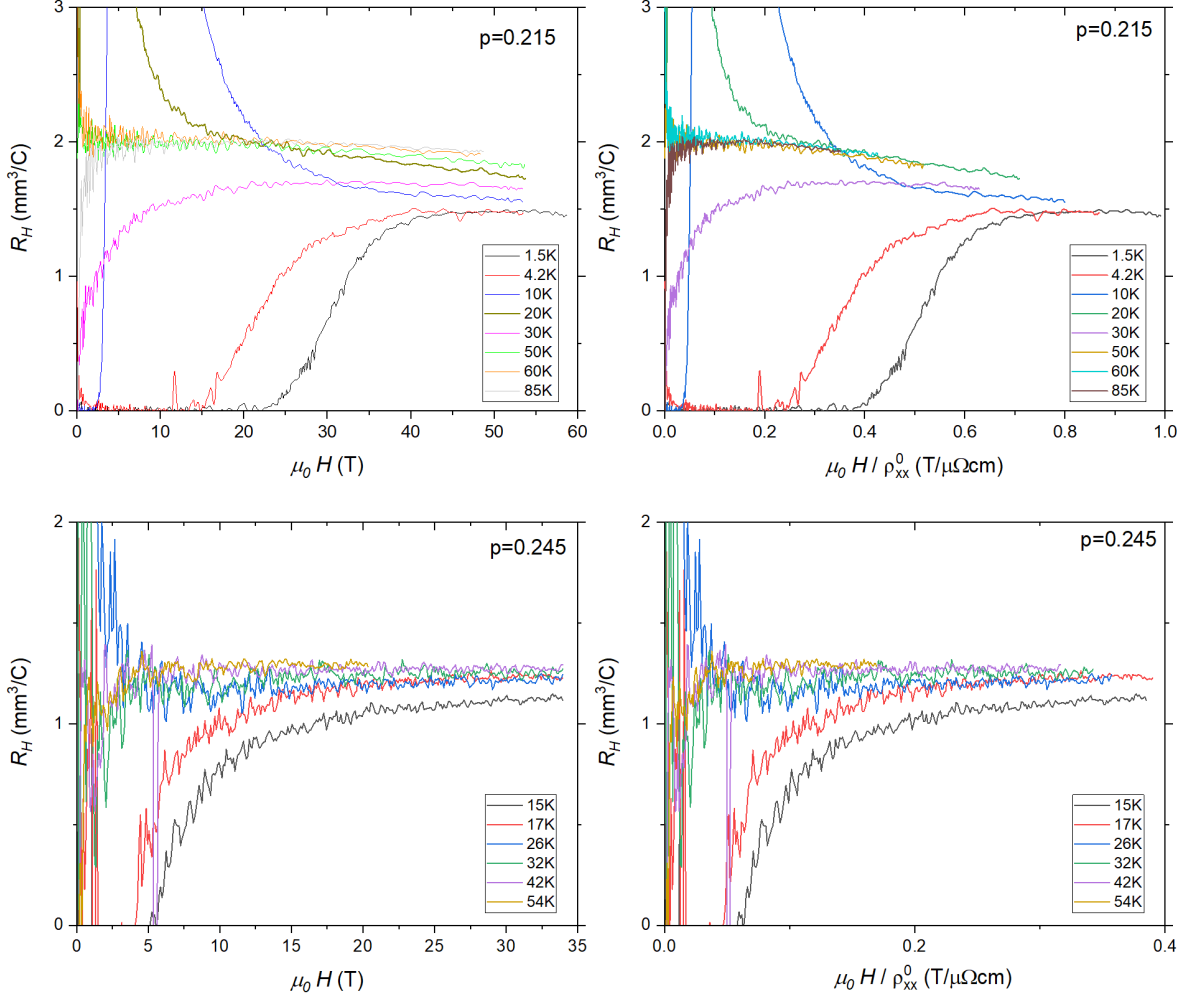


Fig. S 5: Field dependence of  $R_H$  for the Bi2201 samples at the fixed temperatures indicated. Two samples with different dopings are shown as indicated in the panels. As for Figure 1 in the main text, in the right hand panels the magnetic field has been scaled by dividing by the extrapolated zero field resistance at that temperature.

silver paint and annealing at 450°C in flowing oxygen for 10 minutes. Zero-field resistance versus temperature curves were measured in zero field by a standard four-probe ac lock-in detection technique. Measurements of  $R_H$  were performed either in pulsed magnetic fields at the LNCMI in Toulouse or in static fields at the HFML in Nijmegen. As with the Tl2201 study, the Hall resistance  $R_{xy}$  was determined by taking the anti-symmetrised signal from measurements made with the magnetic field applied both parallel and anti-parallel to the  $c$ -axis. Plots of the Hall

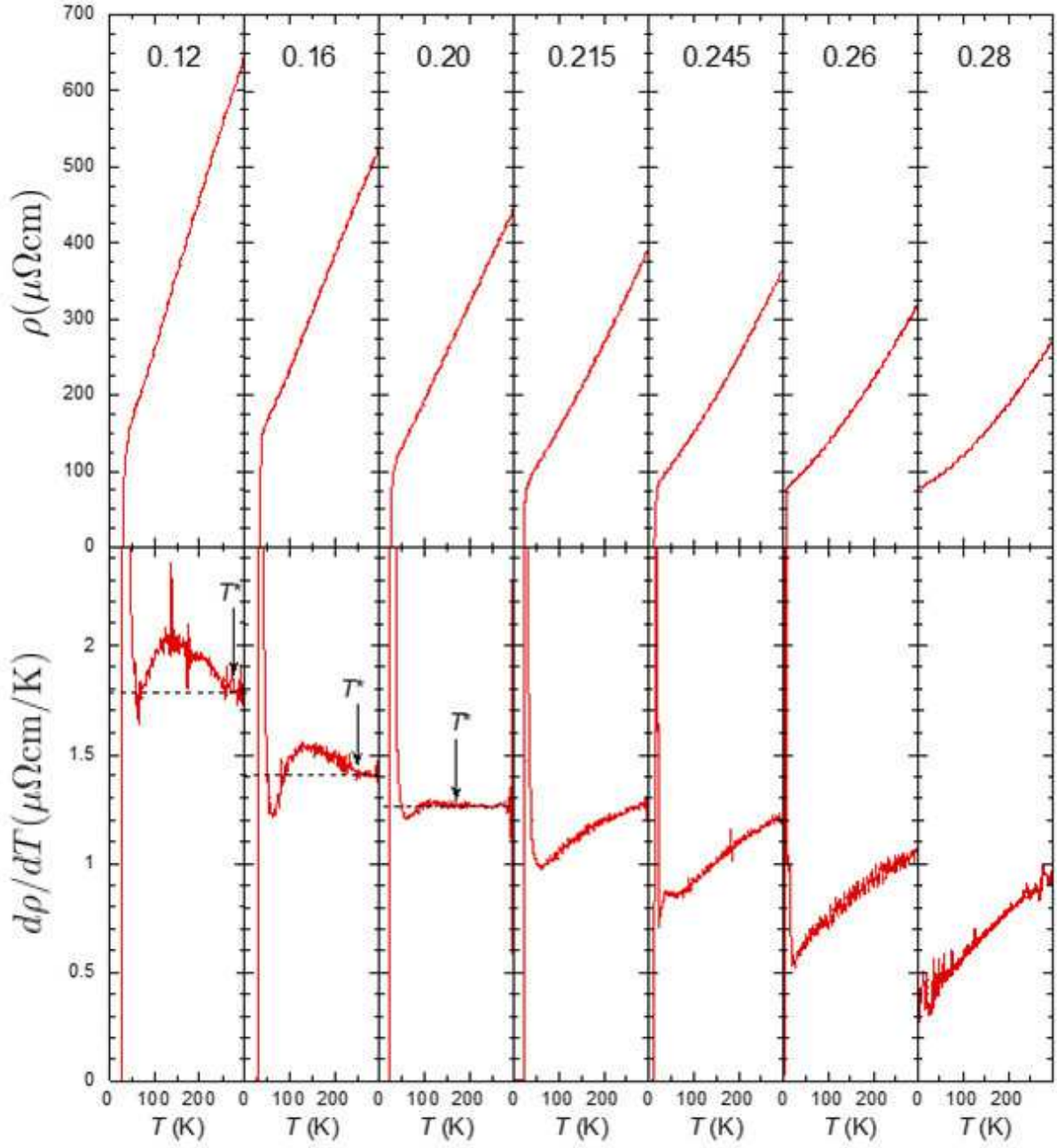


Fig. S 6: Resistivity versus temperature for Bi2201 sample with doping as indicated. The bottom panels show the derivative  $d\rho/dT$ , with the position of the upturn due to the pseudogap indicated. The dashed lines are guides to the eye.

voltage versus field and temperature, similar to Fig. 1 of the main text, are shown in Figure 5.

There is some debate and uncertainty about the precise doping levels for the La-Bi2201 system. However, since the focus of this particular study is on the evolution of the Hall number with doping beyond  $p^*$ , the doping level relative to  $p^*$  is the critical parameter. Here, we use in-plane resistivity measurements to identify unambiguously the location of  $p^*$  within our set of samples. The nominal doping levels for each sample are deduced from these  $T_c$  values using the conventional formula  $T_c/T_c^{\max} = (1 - 82.6(p - 0.16)^2)$ , with  $T_{c,\max} = 34$  K, except for the sample labeled  $p = 0.28$  which has  $T_c < 2$  K. For this sample we use the doping dependence of the linear coefficient of the resistivity ( $A$ ) as

shown in Figure 3 of the main text.

The zero-field resistivity curves for the individual La-Bi2201 crystals are displayed in the top panels of Figure 6. For completeness, we show measurements over the full range of dopings that were available to us in order to highlight the location of  $p^*$ , the critical end point for the pseudogap. In clean, underdoped cuprates, the opening of the normal state pseudogap manifests itself as a downturn in the in-plane resistivity at a temperature  $T^*$  that coincides well with the temperature at which a downturn is also seen in the NMR Knight shift. This downturn in  $\rho_{xx}(T)$  is most readily identified as an upturn in the temperature derivative  $d\rho_{xx}/dT$ . As indicated in the bottom panels of Figure 6, upturns in  $d\rho_{xx}/dT$  are seen for all dopings up to and including  $p = 0.20$ . The upturn for  $p = 0.20$  is small but discernable. Beyond  $p = 0.20$ , however, the  $d\rho_{xx}/dT$  plots exhibit the characteristic shape of other overdoped cuprates such as LSCO and Tl2201. This allow us to clearly pinpoint the end of the pseudogap to be between  $p = 0.20$  and  $p = 0.215$  in this La-Bi2201 system. Estimates for  $A$ , the coefficient of the  $T$ -linear term in the zero-field resistivity, are obtained by extrapolating the slopes in the derivatives  $d\rho_{xx}/dT$  to the zero-temperature axis.

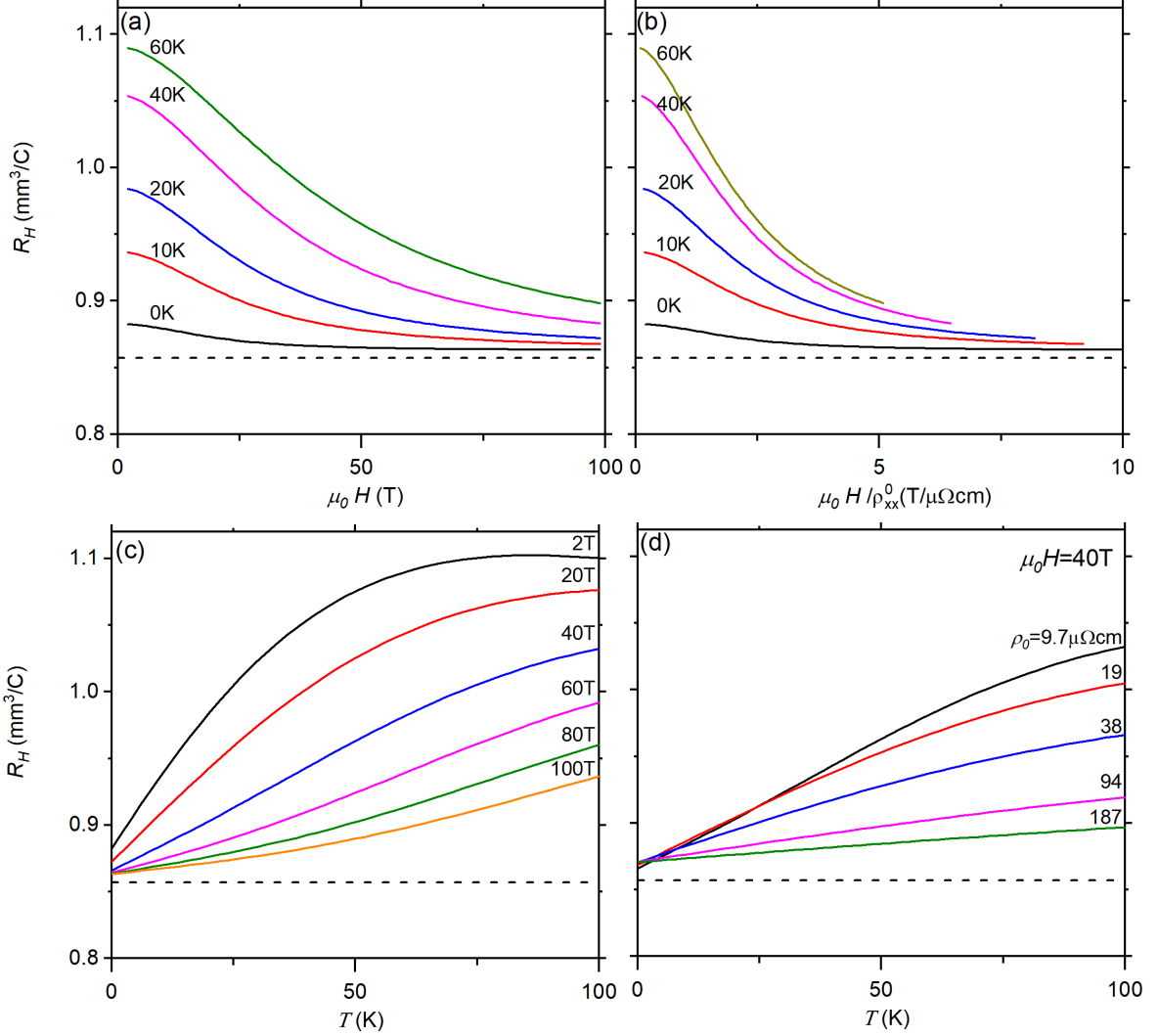


Fig. S 7: Simulation of  $R_H$  for Tl2201, with  $T_c = 20$  K. (a) Field dependence of  $R_H$  at fixed temperatures as indicated. (b) Akin to Kohler's plot  $R_H(B)/\rho_{xx}^0$ . (c) Temperature dependence of  $R_H$  at the fixed fields indicated. (d) Effect of increased impurity scattering on the temperature dependence of  $R_H$  at a fixed field of  $\mu_0 H = 40$  T. The dashed line in all panels indicates the value of  $R_H$  calculated from the expression  $R_H = 1/ne$ , where  $n = \pi k_{F0}^2/(2\pi c)$ .

### Simulation of field and temperature dependence of $R_H$ within Boltzmann transport theory

To understand the evolution of  $R_H$  with field and temperature, we calculated the expected behavior using conventional Boltzmann transport theory and the Fermi surface parameters of Tl2201 which have previously been determined from angle dependent c-axis magnetoresistance (ADMR) measurements. In general, the conductivity tensor can be calculated from the Shockley-Chambers tube-integral formula (SCTIF), generalized for the case where both the Fermi velocity  $v_f$  and the scattering rate vary around the Fermi surface [23]. This is valid for arbitrary field values (i.e., not only in the low or high field limits). For a two-dimensional Fermi surface the SCTIF is given by

$$\sigma_{ij} = \frac{e^3 B}{2\pi^2 \hbar^2 c} \int_0^{2\pi} d\phi \int_0^\infty d\phi' \frac{v_i(\phi) v_j(\phi - \phi')}{\omega_c(\phi) \omega_c(\phi - \phi')} e^{G(\phi - \phi') - G(\phi)} \quad (1)$$

where  $G(\phi) = \int d\phi/[\omega_c(\phi)\tau(\phi)]$ ,  $c$  is the in-plane lattice constant and  $i, j \in (x, y, z)$  and  $\phi$  is the azimuthal angle. For Tl2201, the ADMR data was fitted by assuming  $k_F(\phi) = k_{00} + k_{40} \cos(4\phi)$ ,  $\tau(\phi) = \tau^0/(1 + \gamma \cos 4\phi)$ ; i.e., the first two terms in a cylindrical harmonic expansion of  $k_F(\phi)$  and the four-fold angle dependence to the scattering rate consistent with the crystal symmetry. In the fits, it was not possible to discriminate between the angle dependence of  $\omega_c$  and  $\tau$  so  $\omega_c(\phi)$  was set to be independent of  $\phi$ , and varies linearly with  $H$  ( $\omega_c = \omega_c^0 H$ ) [23]. So the relevant parameters are  $k_{00}$ ,  $k_{40}$ ,  $\omega_c^0 \tau^0(T)$  and  $\gamma(T)$ . Within this approximation

$$\sigma_{ij} = \frac{e^3 B}{2\pi^2 \hbar^2 c \omega_c^2} \int_0^\pi d\phi \int_0^\infty d\phi' v_j(\phi) v_j(\phi - \phi') e^{G(\phi - \phi') - G(\phi)} \quad (2)$$

where  $v_x = k_f(\phi)\omega_c \cos(\phi - \zeta)\hbar/(eB)$ ,  $v_y = k_f(\phi)\omega_c \sin(\phi - \zeta)\hbar/(eB)$  and  $\zeta$  is the angle between  $k_f$  and  $v_f$ ;  $\tan(\zeta) = d \ln k_f(\phi)/d\phi$ . Both  $\sigma_{xx}$  and  $\sigma_{xy}$  are calculated for each temperature point and then  $R_H = -\sigma_{xy}/(\sigma_{xx}^2 + \sigma_{xy}^2)B$ .  $\omega_c^0 \tau^0(T)$  and  $\gamma(T)$  are related to the anisotropic and isotropic components of the scattering rate which were found to have linear and quadratic temperature dependencies respectively;  $(1 - \gamma)/(\omega_c^0 \tau^0) = A_{iso} + B_{iso} T^2$  and  $2\gamma/\omega_c^0 \tau^0 = A_{ani} + B_{ani} T$ .

Parameter	Value
$k_{00}$	$0.728 \text{ \AA}^{-1}$
$k_{40}/k_{00}$	$-3.3 \times 10^{-2}$
$A_{iso}$	2.43
$B_{iso}$	$3.13 \times 10^{-4}$
$A_{ani}$	0.135
$B_{ani}$	$6.11 \times 10^{-2}$

Table S III: Parameters derived from ADMR fits used for the magneto-transport calculations (sample tl200c1 from Ref. [44]) valid for  $T \leq 70$  K and at  $\mu_0 H = 45$  T.

Results of the calculations using the parameters derived from ADMR fits to a  $T_c = 20$  K sample of Tl2201 [44] (parameters given in Table S), are shown in Figure 7. In panel (a) of Figure 7 the field dependence of  $R_H$  at different temperatures is seen to closely resemble the experimental behaviour seen in Figure 1 of the main text. There is a monotonic decrease of  $R_H$  as the field is increased with  $R_H$  tending towards  $1/ne$  at the highest fields. This is emphasized in panel (b) of the same figure. In simple metals, all components of the magnetoresistance tensor should fall onto a common curve when plotted as a function of  $\omega_c \tau$ , and which is proportional to the  $H/\rho_{xx}^0$ , where  $\rho_{xx}^0$  is the longitudinal resistance in zero field. In Tl2201, this behaviour, which is known as Kohler's rule, is not expected because the *anisotropy* of the scattering rate is temperature dependent. The  $R_H(B)$  values do not collapse onto a common curve but can be seen to approach a common limiting value at high field. At the lowest temperature there remains some small field dependence of  $R_H$  because of the non-circular shape of the Fermi surface.  $R_H$  does not exactly equal  $1/ne$  for either an isotropic scattering rate or an isotropic mean-free-path in the low field limit, however, the deviations for the Fermi surface parameters of Tl2201 are small.

In panel (c) of Figure 7, we show how the temperature dependence of  $R_H$  evolves with field. At higher field the temperature dependence of  $R_H$  is much weaker, and it is easier to extrapolate to the zero temperature limit where

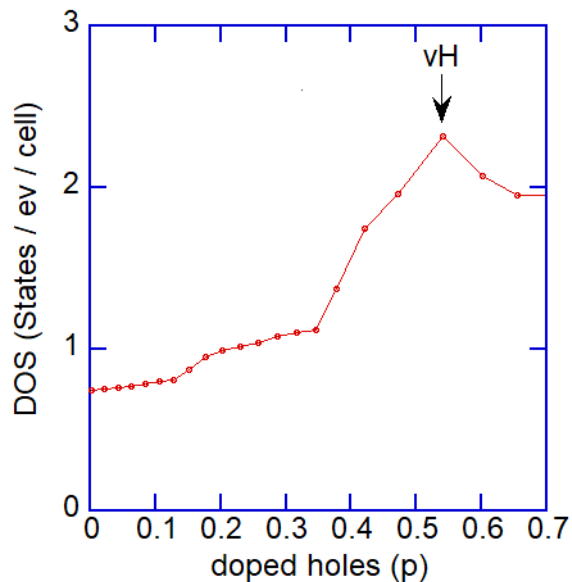


Fig. S 8: DFT calculation of density of state for Tl2201, plotted versus doping  $p$ . The van Hove point where the Fermi surface undergoes a Lifshitz transition is marked vH.

$R_H$  is close to  $1/ne$ . Finally, in panel (d) we show the effect of increased impurity scattering which is relevant for the interpretation of the  $R_H$  data of Bi2201. Here we have increased  $A_{iso}$  which has the effect of increasing the residual resistance value  $\rho_0$ . The figure shows that at a fixed field of 40 T the effect of the increased impurity scattering is to strongly suppress the temperature dependence of  $R_H$ . Hence, although the values of  $\omega_c\tau$  will be lower for less pure samples, the value of  $R_H$  still is close to  $1/ne$ .

**Lifshitz transition in Tl2201** Density functional theory (DFT) has been found to provide an excellent description of the electronic structure of Tl2201 close to the Fermi level [6]. In Fig. S8 we show the density of states of Tl2201, calculated using DFT as described in Ref. [6], plotted against doping within a rigid band model. At low doping, the Fermi surface is closed around the  $M$  point in the Brillouin zone, however for  $p \gtrsim 0.5$  the Fermi surface becomes closed around the  $\Gamma$  point. This Lifshitz transition results in a peak in the density of states and is labelled vH in the figure. A similar Lifshitz transition occurs in all cuprates, but unlike in LSCO and Nd-LSCO, in Tl2201 it occurs for  $p$  much larger than the range for which superconductivity is observed. This is consistent with the fact that  $R_H$  remains positive throughout the doping range we have measured in our study.

- 
- [1] B. Keimer, S. A. Kivelson, M. R. Norman, S. Uchida, and J. Zaanen, From quantum matter to high-temperature superconductivity in copper oxides, *Nature* **518**, 179 (2015).
  - [2] D. LeBoeuf, N. Doiron-Leyraud, J. Levallois, R. Daou, J. B. Bonnemaïson, N. E. Hussey, L. Balicas, B. J. Ramshaw, R. X. Liang, D. A. Bonn, W. N. Hardy, S. Adachi, C. Proust, and L. Taillefer, Electron pockets in the fermi surface of hole-doped high- $t_c$  superconductors, *Nature* **450**, 533 (2007).
  - [3] S. E. Sebastian, N. Harrison, and G. G. Lonzarich, Towards resolution of the fermi surface in underdoped high- $t_c$  super-

- conductors, Rep. Prog. Phys. **75**, 102501 (2012).
- [4] B. Vignolle, A. Carrington, R. A. Cooper, M. M. J. French, A. P. Mackenzie, C. Jaudet, D. Vignolles, C. Proust, and N. E. Hussey, Quantum oscillations in an overdoped high- $t_c$  superconductor, Nature **455**, 952 (2008).
- [5] A. F. Bangura, P. M. C. Rourke, T. M. Benseman, M. Matusiak, J. R. Cooper, N. E. Hussey, and A. Carrington, Fermi surface and electronic homogeneity of the overdoped cuprate superconductor  $\text{t}_2\text{ba}_2\text{cuo}_{6+\delta}$  as revealed by quantum oscillations, Phys. Rev. B **82**, 140501 (2010).
- [6] P. M. C. Rourke, A. F. Bangura, T. M. Benseman, M. Matusiak, J. R. Cooper, A. Carrington, and N. E. Hussey, A detailed de haas-van alphen effect study of the overdoped cuprate  $\text{t}_2\text{ba}_2\text{cuo}_{6+\delta}$ , New J. Phys. **12**, 105009 (2010).
- [7] N. E. Hussey, M. Abdel-Jawad, A. Carrington, A. P. Mackenzie, and L. Balicas, A coherent three-dimensional fermi surface in a high-transition-temperature superconductor, Nature **425**, 814 (2003).
- [8] M. Plate, J. D. F. Mottershead, I. S. Elfimov, D. C. Peets, R. Liang, D. A. Bonn, W. N. Hardy, S. Chiuzbaian, M. Falub, M. Shi, L. Patthey, and A. Damascelli, Fermi surface and quasiparticle excitations of overdoped  $\text{t}_2\text{ba}_2\text{cuo}_{6+\delta}$ , Phys. Rev. Lett. **95**, 077001 (2005).
- [9] Y. Kubo, Y. Shimakawa, T. Manako, and H. Igarashi, Transport and magnetic-properties of  $\text{t}_2\text{ba}_2\text{cuo}_{6+\delta}$  showing a delta-dependent gradual transition from an 85 k superconductor to a nonsuperconducting metal, Phys. Rev. B **43**, 7875 (1991).
- [10] T. Manako, Y. Kubo, and Y. Shimakawa, Transport and structural study of  $\text{t}_2\text{ba}_2\text{cuo}_{6+\delta}$  single-crystals prepared by the kcl flux method, Phys. Rev. B **46**, 11019 (1992).
- [11] N. E. Hussey, Phenomenology of the normal state in-plane transport properties of high- $t_c$  cuprates, J. Phys.-Condens. Matter **20**, 123201 (2008).
- [12] N. E. Hussey, H. Gordon-Moys, J. Kokalj, and R. H. McKenzie, Generic strange-metal behaviour of overdoped cuprates, J. Phys.: Conf. Ser. **449**, 012004 (2013).
- [13] T. Shibauchi, A. Carrington, and Y. Matsuda, A quantum critical point lying beneath the superconducting dome in iron pnictides, Annu. Rev. Condens. Matter Phys. **5**, 113 (2014).
- [14] L. Taillefer, Scattering and pairing in cuprate superconductors, Annu. Rev. Condens. Matter Phys. **1**, 51 (2010).
- [15] S. Blanco-Canosa, A. Frano, E. Schierle, J. Porras, T. Loew, M. Minola, M. Bluschke, E. Weschke, B. Keimer, and M. Le Tacon, Resonant x-ray scattering study of charge-density wave correlations in  $\text{yba}_2\text{cu}_3\text{o}_{6+x}$ , Phys. Rev. B **90**, 054513 (2014).
- [16] W. Tabis, B. Yu, I. Bialo, M. Bluschke, T. Kolodziej, A. Kozłowski, E. Blackburn, K. Sen, E. M. Forgan, M. v. Zimmermann, Y. Tang, E. Weschke, B. Vignolle, M. Hepting, H. Gretarsson, R. Sutarto, F. He, M. Le Tacon, N. Barišić, G. Yu, and M. Greven, Synchrotron x-ray scattering study of charge-density-wave order in  $\text{hgba}_2\text{cuo}_{4+\delta}$ , Phys. Rev. B **96**, 134510 (2017).
- [17] J. R. Cooper, J. W. Loram, I. Kokanovic, J. G. Storey, and J. L. Tallon, Pseudogap in  $\text{yba}_2\text{cu}_3\text{o}_{6+\delta}$  is not bounded by a line of phase transitions: Thermodynamic evidence, Phys. Rev. B **89**, 201104 (2014).
- [18] B. J. Ramshaw, S. E. Sebastian, R. D. McDonald, J. Day, B. S. Tan, Z. Zhu, J. B. Betts, R. X. Liang, D. A. Bonn, W. N. Hardy, and N. Harrison, Quasiparticle mass enhancement approaching optimal doping in a high- $t_c$  superconductor, Science **348**, 317 (2015).
- [19] S. Badoux, W. Tabis, F. Laliberte, G. Grissonnanche, B. Vignolle, D. Vignolles, J. Beard, D. A. Bonn, W. N. Hardy, R. Liang, N. Doiron-Leyraud, L. Taillefer, and C. Proust, Change of carrier density at the pseudogap critical point of a cuprate superconductor, Nature **531**, 210 (2016).
- [20] C. Collignon, S. Badoux, S. A. A. Afshar, B. Michon, F. Laliberte, O. Cyr-Choiniere, J. S. Zhou, S. Licciardello, S. Wied-

- mann, N. Doiron-Leyraud, and L. Taillefer, Fermi-surface transformation across the pseudogap critical point of the cuprate superconductor  $\text{La}_{1.6-x}\text{Nd}_{0.4}\text{Sr}_x\text{CuO}_4$ , *Phys. Rev. B* **95**, 224517 (2017).
- [21] C. Putzke, L. Malone, S. Badoux, B. Vignolle, D. Vignolles, W. Tabis, P. Walmsley, M. Bird, N. E. Hussey, C. Proust, and A. Carrington, Inverse correlation between quasiparticle mass and  $t_c$  in a cuprate high- $t_c$  superconductor, *Sci. Adv.* **2**, e1501657 (2016).
- [22] C. E. Matt, C. G. Fatuzzo, Y. Sassa, M. Månsson, S. Fatale, V. Bitetta, X. Shi, S. Pailhès, M. H. Berntsen, T. Kurosawa, M. Oda, N. Momono, O. J. Lipscombe, S. M. Hayden, J.-Q. Yan, J.-S. Zhou, J. B. Goodenough, S. Pyon, T. Takayama, H. Takagi, L. Patthey, A. Bendounan, E. Razzoli, M. Shi, N. C. Plumb, M. Radovic, M. Grioni, J. Mesot, O. Tjernberg, and J. Chang, Electron scattering, charge order, and pseudogap physics in  $\text{La}_{1.6-x}\text{Nd}_{0.4}\text{Sr}_x\text{CuO}_4$ : An angle-resolved photoemission spectroscopy study, *Phys. Rev. B* **92**, 134524 (2015).
- [23] M. Abdel-Jawad, M. P. Kennett, L. Balicas, A. Carrington, A. P. Mackenzie, R. H. McKenzie, and N. E. Hussey, Anisotropic scattering and anomalous normal-state transport in a high-temperature superconductor, *Nat. Phys.* **2**, 821 (2006).
- [24] M. Abdel-Jawad, J. G. Analytis, L. Balicas, A. Carrington, J. P. H. Charmant, M. M. J. French, and N. E. Hussey, Correlation between the superconducting transition temperature and anisotropic quasiparticle scattering in  $\text{t}_2\text{ba}_2\text{cuo}_{6+\delta}$ , *Phys. Rev. Lett.* **99**, 107002 (2007).
- [25] T. Kondo, T. Takeuchi, U. Mizutani, T. Yokoya, S. Tsuda, and S. Shin, Contribution of electronic structure to thermoelectric power in  $(\text{Bi,Pb})_2(\text{Sr,L a})_2\text{CuO}_{6+\delta}$ , *Phys. Rev. B* **72**, 024533 (2005).
- [26] T. Kondo, T. Takeuchi, A. Kaminski, Y. Tsuda, and S. Shin, Evidence for two energy scales in the superconducting state of optimally doped  $(\text{Bi,Pb})_2(\text{Sr,L a})_2\text{CuO}_{6+\delta}$ , *Phys. Rev. Lett.* **98**, 267004 (2007).
- [27] W. D. Wise, M. C. Boyer, K. Chatterjee, T. Kondo, T. Takeuchi, H. Ikuta, Y. Wang, and E. W. Hudson, Charge-density-wave origin of cuprate checkerboard visualized by scanning tunnelling microscopy, *Nat. Phys.* **4**, 696 (2008).
- [28] W. D. Wise, K. Chatterjee, M. C. Boyer, T. Kondo, T. Takeuchi, H. Ikuta, Z. Xu, J. Wen, G. D. Gu, Y. Wang, and E. W. Hudson, Imaging nanoscale fermi-surface variations in an inhomogeneous superconductor, *Nat. Phys.* **5**, 213 (2009).
- [29] T. Kondo, R. Khasanov, T. Takeuchi, J. Schmalian, and A. Kaminski, Competition between the pseudogap and superconductivity in the high- $t_c$  copper oxides, *Nature* **457**, 296 (2009).
- [30] F. Balakirev, J. Betts, A. Migliori, S. Ono, Y. Ando, and G. Boebinger, Signature of optimal doping in hall-effect measurements on a high-temperature superconductor, *Nature* **424**, 912 (2003).
- [31] D. Pelc, P. Popčević, M. Požek, M. Greven, and N. Barišić, Unusual behavior of cuprates explained by heterogeneous charge localization, *Science Advances* **5**, eaau4538 (2019).
- [32] J. M. Wade, J. W. Loram, K. A. Mirza, J. R. Cooper, and J. L. Tallon, Electronic specific-heat of  $\text{t}_2\text{ba}_2\text{cuo}_{6+\delta}$  from 2 k to 300 k for  $0 \geq \delta \geq 0.1$ , *J. Supercond.* **7**, 261 (1994).
- [33] J. M. Tallon, J. G. Storey, J. R. Cooper, and J. W. Loram, Locating the pseudogap closing point in cuprate superconductors: absence of entrant or reentrant behavior, *arXiv:1907.12018* (2019).
- [34] D. M. Broun, D. C. Morgan, R. J. Ormeno, S. F. Lee, A. W. Tyler, A. P. Mackenzie, and J. R. Waldram, In-plane microwave conductivity of the single-layer cuprate  $\text{t}_2\text{ba}_2\text{cuo}_{6+\delta}$ , *Phys. Rev. B* **56**, R11443 (1997).
- [35] E. Abrahams and C. M. Varma, Hall effect in the marginal fermi liquid regime of high- $t_c$  superconductors, *Phys. Rev. B* **68**, 094502 (2003).
- [36] Y. Ding, L. Zhao, H.-T. Yan, Q. Gao, J. Liu, C. Hu, J.-W. Huang, C. Li, Y. Xu, Y.-Q. Cai, H.-T. Rong, D.-S. Wu, C.-Y. Song, H.-X. Zhou, X.-L. Dong, G.-D. Liu, Q.-Y. Wang, S.-J. Zhang, Z.-M. Wang, F.-F. Zhang, F. Yang, Q.-J. Peng, Z.-Y. Xu, C.-T. Chen, and X. J. Zhou, Disappearance of superconductivity and a concomitant lif

- shitz transition in heavily overdoped  $\text{Bi}_2\text{Sr}_2\text{CuO}_6$  superconductor revealed by angle-resolved photoemission spectroscopy, *Chinese Phys. Lett.* **36**, 017402 (2019).
- [37] D. Deepwell, D. C. Peets, C. J. S. Truncik, N. C. Murphy, M. P. Kennett, W. A. Huttema, R. Liang, D. A. Bonn, W. N. Hardy, and D. M. Broun, Microwave conductivity and superfluid density in strongly overdoped  $\text{t}_2\text{ba}_2\text{cuo}_{6+\delta}$ , *Phys. Rev. B* **88**, 214509 (2013).
- [38] R. A. Cooper, Y. Wang, B. Vignolle, O. J. Lipscombe, S. M. Hayden, Y. Tanabe, T. Adachi, Y. Koike, M. Nohara, H. Takagi, C. Proust, and N. E. Hussey, Anomalous criticality in the electrical resistivity of  $\text{La}_{2-x}\text{Sr}_x\text{CuO}_4$ , *Science* **323**, 603 (2009).
- [39] A. Legros, S. Benhabib, W. Tabis, F. Laliberte, M. Dion, M. Lizaire, B. Vignolle, D. Vignolles, H. Raffy, Z. Z. Li, P. Auban-Senzier, N. Doiron-Leyraud, P. Fournier, D. Colson, L. Taillefer, and C. Proust, Universal t-linear resistivity and planckian dissipation in overdoped cuprates, *Nature Physics* **15**, 142 (2019).
- [40] M. M. J. French, J. G. Analytis, A. Carrington, L. Balicas, and N. E. Hussey, Tracking anisotropic scattering in overdoped  $\text{t}_2\text{ba}_2\text{cuo}_{6+\delta}$  above 100 k, *New J. Phys.* **11**, 055057 (2009).
- [41] A. P. Mackenzie, S. R. Julian, D. C. Sinclair, and C. T. Lin, Normal-state magnetotransport in superconducting  $\text{t}_2\text{ba}_2\text{cuo}_{6+\delta}$  to millikelvin temperatures, *Phys. Rev. B* **53**, 5848 (1996).
- [42] A.W. Tyler, An Investigation into the Magnetotransport Properties of Layered Superconducting Perovskites. Ph.D. thesis, University of Cambridge (1997).
- [43] R. Liang, D. A. Bonn, and W. N. Hardy, Evaluation of  $\text{CuO}_2$  plane hole doping in  $\text{YBa}_2\text{Cu}_3\text{O}_{6+x}$  single crystals, *Phys. Rev. B* **73**, 180505 (2006).
- [44] M. French, PhD Thesis University of Bristol (2009).

